Hindawi
Advances in Condensed Matter Physics
Volume 2023, Article ID 7369790, 10 pages
https://doi.org/10.1155/2023/7369790

Research Article

Tailoring Multiferroic Characteristics in $LaFeO_3$ Nanocrystals via Rare-Earth Pr^{3+} Doping

Ramesh Kumar Raji,[1] **Tholkappiyan Ramachandran**,[2,3] **Fathalla Hamed**,[2] **and Srinivasa S**[1]

[1]*Department of Physics, Surana College (Autonomous), South End Road, Bangalore, Karnataka 560004, India*
[2]*Department of Physics, College of Science, United Arab Emirates University, P.O. Box-15551, Al Ain, UAE*
[3]*National Water and Energy Center, United Arab Emirates University, P.O. Box-15551, Al Ain, UAE*

Correspondence should be addressed to Ramesh Kumar Raji; ramesh.phy@suranacollege.edu.in

Received 9 October 2023; Revised 10 November 2023; Accepted 24 November 2023; Published 9 December 2023

Academic Editor: Ashwini Kumar

Multiferroic materials have sparked significant interest in the realm of materials science because of their potential impact on various device applications. This study focuses on the synthesis of nanocrystalline $La_{1-x}Pr_xFeO_3$ (LPFO) materials, where x can be either 0 or 0.5, using a solid-state technique. The aim is to gain insights into their structural, optical, dielectric, and magnetic properties. To confirm the chemical phase of the synthesized materials, X-ray diffractometer and Raman spectroscopy were employed. The outcome of the Rietveld analysis reveals that the LPFO crystallites exhibit orthorhombic symmetry with a Pbnm space group. The functional groups that were present in the LPFO samples were identified using FT-IR spectroscopic analysis. The morphological studies using scanning electron microscope and transmission electron microscope indicate that the synthesized samples exhibit excellent homogeneity with uniformly distributed grains. In order to investigate the dielectric constant (ε') and dielectric loss ($\tan\delta$) were examined as functions of temperature and frequency. Pr^{3+} dopants had a notable impact on the dielectric characteristics, particularly within the frequency span of 10 kHz–1 MHz and over the temperature variation of 40–160°C. The ambient temperature magnetic properties of the LPFO ferrite materials displayed antiferromagnetic behavior. Ultimately, this research reveals insightful information on the structural, optical, dielectric, and magnetic properties of the synthesized nanocrystalline LPFO materials, shedding light on their potential applications in the multifunctional devices.

1. Introduction

The perovskite-type ferrite material with the general formula ABO_3, known for its stability, has garnered significant attention from researchers in the field of nanotechnology. Among the various nanosized ferrites, ABO_3-type rare-earth orthoferrites, such as $LaFeO_3$, stand out as particularly intriguing materials due to their diverse set of properties, including optical, electronic, catalytic, ferroelectric, and magnetic characteristics. These properties make $LaFeO_3$ highly versatile and suitable for applications in photocatalysts, biosensors, solid oxide fuel cells, photovoltaic cells, and magnetic data storage [1–3]. At room temperature, $LaFeO_3$ exhibits antiferromagnetic behavior and acts as an insulator with a Neel temperature of 740 K [4]. When scaled down to the nanoscale, $LaFeO_3$ demonstrates exceptional characteristics, including enhanced sensing properties, a larger surface area, and improved catalytic activity, thanks to the quantum size effect. In the literature, several synthesis methods have been reported for producing nanocrystalline $LaFeO_3$ materials, including the coprecipitation method [5], microemulsion method [6], electrospinning technique [7], hot soap method [8], hydrothermal method [9], polymer pyrolysis method [10], thermal decomposition method [11], and auto-combustion technique [12]. Each of these methods offers its own set of advantages, disadvantages, and limitations. However, the traditional high-temperature or the approach of solid-state reaction technique has gained significant attention due to its simplicity, high reactivity, and cost-effectiveness in the production of nanocrystalline materials. This method remains a preferred choice for synthesizing $LaFeO_3$ nanocrystals.

Currently, researchers have become more interested in examining the effects of rare-earth element substitutions in ferrite materials. Remarkably, the perovskite structure of

$LaFeO_3$ demonstrates a remarkable tolerance for a wide range of dopant ions. This flexibility allows researchers to precisely tailor and control the properties of the final product based on the type and concentration of the dopant used. The physicochemical characteristics of $LaFeO_3$ can be finely tuned by selecting specific synthesis methods and carefully controlling the amount of dopant incorporated. Various dopants have been employed to occupy either the A or B sites within the $LaFeO_3$ structure, resulting in alterations in the material's band gaps, morphology, cell characteristics, crystalline size, and grain diameters. These modifications can be harnessed for various applications. In recent studies, conventional solid-state techniques were utilized to synthesize compounds like Sm/Nd-doped $LaFeO_3$ ($La_{0.9}(Sm/Nd)_{0.1}FeO_3$), Co-doped $LaFeO_3$ ($LaCo_xFe_{1-x}O_3$, where $x = 0.05$, 0.1, 0.15, 0.2, 0.25), Ti-doped $LaFeO_3$ ($LaTi_xFe_{1-x}O_3$, where $x = 0$, 0.05, 0.15, 0.25), and Mn-doped $LaFeO_3$ ($LaMn_xFe_{1-}O_3$, where $x = 0.05$, 0.1, 0.15, 0.2, 0.25) [13, 14]. These nanocrystalline compounds were successfully synthesized using oxide materials as starting precursors and showed promise in applications such as gas sensing, magnetic memory storage, high-frequency switching, and more. Additionally, compounds like $La_{0.9}M_{0.1}FeO_3$ (M = Ca and Ba) were explored as thermoelectric materials, and have potential uses in power generation, waste heat recovery, and refrigeration [15]. Moreover, recently Kumar et al. [16] have been synthesized using the sol–gel method, multiferroic $BiFeO_3$—NiO (BFO—NiO) nanocomposites have been created and studied. The stability and physical characteristics of the solid state-synthesized lead-free K, Na, and Nb-doped $BiFeO_3$ system have been demonstrated by Reygadas et al. [17]. Comparative evaluation of $BiFeO_3$-modified devices based on "La" for high-conversion efficiency perovskite solar cells have been developed by Raj et al. [18]. The structural, dielectric, transport, and ferroelectric properties of Ca-Modified $Bi_{0.80}La_{0.20}FeO_3$ (BCLFO) polycrystalline samples produced by the solid-state reaction are investigated by Kumar et al. [19]. Using the sol–gel combustion method, nanoparticles (NPs) of $(La_{1-x}Sr_x)(Fe_{1-x}Ni_x)O_3$, ($x = 0.0$, 0.1, and 0.2), with an orthorhombic perovskite structure, were successfully prepared by Saad et al. [20]. Redistributing dissolved Cu nanoparticles on $LaFeO_3$ photocatalyst for adjustable CO_2 reduction through photocatalysis has been demonstrated by Saad et al. [21]. Ni doping's effect on the physical characteristics of $La_{0.7}Sr_{0.3}FeO_3$ produced using the reverse micelle technique reported by Hassan et al. [22].

Continuing this line of research on $LaFeO_3$ materials, the current study investigates the incorporation of Pr^{3+} as a dopant to replace rare-earth A-site (La) ions in $LaFeO_3$. The aim is to explore and understand the intrinsic properties of the resulting materials. As far as we are aware, there have not been any prior investigations into the effects of Pr^{3+} substitution in $LaFeO_3$ using conventional solid-state techniques. This research seeks to fill this gap in our understanding of these materials.

In this study, our primary objective is to document the synthesis of $La_{1-x}Pr_xFeO_3$ (LPFO) materials, where x can be either 0 or 0.5, using the conventional solid-state technique. What sets this research apart is its focus on understanding the impact of substituting rare-earth Pr^{3+} ions into the nanocrystalline $LaFeO_3$ material. Specifically, we aim to investigate how this substitution has an impact on the structural, morphological, dielectric, and magnetic characteristics of nanoscale $LaFeO_3$. To achieve this goal, we have undertaken a comprehensive characterization of the synthesized nanocrystalline $LaFeO_3$ materials. Our analytical techniques include X-ray diffractometer (XRD), FT-IR (Fourier Transform-Infrared spectroscopy), the Raman spectroscopy method, scanning electron microscope (SEM) coupled to energy dispersive X-ray spectrometry (EDS), transmission electron microscope (TEM), measurements of the dielectric constant and loss, and magnetic property analysis using a vibrating sample magnetometer (VSM). Through these investigations, we seek to provide insights into how the presence of Pr^{3+} ions influences the intrinsic properties of the nanocrystalline LPFO ferrite material.

2. Experimental Section

2.1. Synthesis Materials and Technique. Praseodymium oxide (Pr_6O_{11}), Lanthanum (III) oxide (La_2O_3), and Iron oxide (Fe_2O_3) precursors with purity of 99.9%, sourced from Sigma–Aldrich, served as the initial materials. The nanocrystalline compounds, denoted as $La_{1-x}Pr_xFeO_3$ (LPFO) with x values of 0 and 0.5, were fabricated using the traditional high-temperature solid-state reaction technique. To achieve a uniform fine powder, the chosen initial materials were carefully weighed in the required stoichiometric ratio and powdered for ~1.5 hr using an agate mortar.

Subsequently, the powders underwent calcination at 900°C for a duration of 12 hr, followed by thorough grinding. Following that, they were then placed into an alumina container. In addition, the processing involved sintering the samples at 1100°C for 6 hr, with intermittent crushing steps. The resultant synthesized ferrite powders allowed to achieve homogeneity, the mixture should progressively come down to room temperature at a pace of 5°C/min. At Final, the prepared LPFO powder samples were subjected to a final sintering step at 1100°C for 6 hr to facilitate phase formation. After this, they were well-grounded and ready for various analytical measurements. To facilitate dielectric characteristics, using a hydraulic press, the prepared ferrite powders were pelletized at a pressure of ~2.5–4.5 tonnes. The schematic diagram depicting the synthesized LPFO ferrite materials schematic diagram is provided in Figure 1.

2.2. Characterization Techniques. The phase and construction of structure composition of the nanocrystalline materials synthesized were investigated using a Bruker D2 phaser XRD, utilizing Cu-Kα (1.5418 Å) radiation. XRD patterns in the 2θ range covering 20–60° were captured. Phase identifications were matched to the PDF-4 database maintained by the International Centre for Diffraction Data (ICDD). Further structural details, including bond angles and bond lengths, were determined through Rietveld refinement using the FULLPROF software package of the recorded XRD profiles. For the additional characterizations, using a Bruker Alpha FTIR Spectrophotometer, FT-IR spectra were acquired

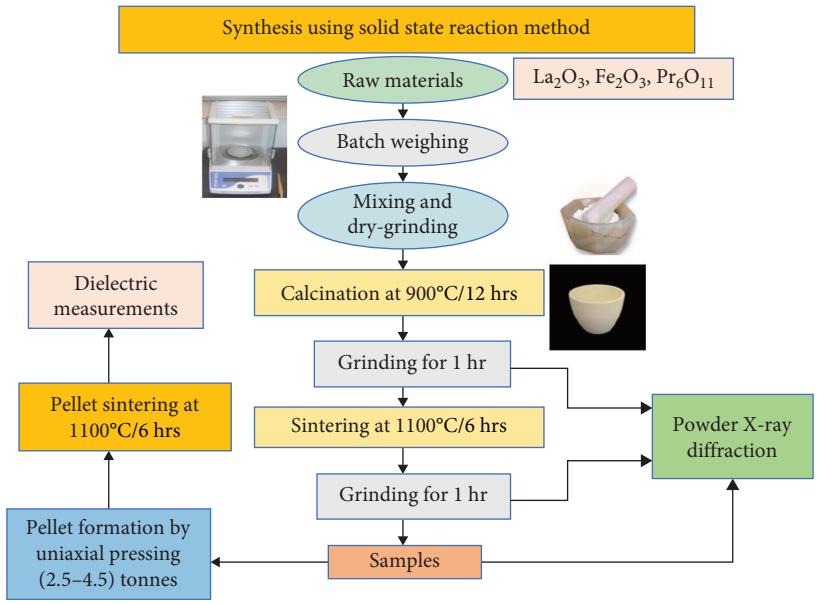

Figure 1: Schematic representation of traditional solid-state reaction synthesized LPFO ferrite nanopowder materials.

in the wavelength spanning 500–1750 cm^{-1}. With the use of a He-Ne laser and a Horiba Jobin-Yvon HR-800 UV Spectrophotometer, room-temperature Raman spectra were obtained that ranged from 100 to 1000 cm^{-1}. A JEOL-ZEM SEM with an energy-dispersive spectrometer (EDX) was used to analyze the surface morphology, elemental distribution mapping, and quantitative assessments of the generated samples. Furthermore, dielectric measurements were performed to assess the temperature and frequency-dependent dielectric properties. These characteristics were measured using a Wayne Kerr—LCR 4275 in the frequency ranges from 10 Hz to 1 MHz. In last, magnetic properties were investigated using a Lakeshore (MODEL-7407) VSM at ambient temperature.

3. Results and Discussion

3.1. Structural Analysis—X-Ray Diffractometer (XRD) Studies. The phase formation of the nanocrystalline LPFO materials that were synthesized was examined using X-ray diffraction. In Figure 2, you can see the XRD pattern obtained through Rietveld refinement of these materials, which were synthesized through the traditional high-temperature solid-state reaction method. This pattern reveals that the diffraction peaks corresponding to the (101), (121), (220), (202), (311), (240), (242), and (204) planes closely matched the ICDD No. 37-1493 database, indicating that the causes of these peaks are the distorted orthorhombic structure of $LaFeO_3$ with the space group of (Pbnm). The refined crystallographic parameters are provided in Table 1. After substituting Pr^{3+} for La in $LaFeO_3$, small discrepancies in bond distances and lattice constraints were measured. The lattice expansion or contraction is to blame for this disparity, which occurs owing to differences in the ionic radii of the host and substituent atoms within the crystal structure. Importantly, there were no additional or impurity peaks were detected in the XRD pattern. This suggests the high purity of the nanocrystalline LPFO materials synthesized materials. The broadening of the diffraction peaks in the XRD pattern indicates that the crystallites within the synthesized materials are relatively small in size. Scherrer's formula was used for estimating the mean size of the crystallite (indicated as "d") of the nanocrystalline LPFO materials. The result is demonstrated by the equation [23] as follows:

$$d = 0.9\lambda/(\beta\cos\theta), \tag{1}$$

where d-is the mean crystallite size, θ-is the angle of diffraction, λ-is the wavelength of the X-ray beam (0.154 nm), and β-is the full-width at half maximum (FWHM). It is perceived that the mean crystallite size (d) of the produced nanocrystalline LPFO materials was about 88 and 65 nm. The diminution in the mean crystallite size can be attributed to the impediment of diffusivity resulting from the substitution of rare-earth element Pr^{3+} into lanthanum ferrite. The dislocation density (represented as "δ"), which quantifies the length of dislocation lines within a crystal per cubic inch, provides a measure of the number of imperfections present in the crystal structure. Utilizing, the formula dislocation density (δ) was calculated [24] as follows:

$$\delta = 1/d^2, \tag{2}$$

where d-is the mean crystallite size. The computed dislocation density values are 12.92×10^{15} lines/m^2 for the synthesized nanocrystalline $LaFeO_3$ and 23.66×10^{15} lines/m^2 for $La_{0.5}Pr_{0.5}FeO_3$ ferrite materials. This increase in δ clearly indicates the successful substitution of Pr^{3+} into the $LaFeO_3$ ferrite materials.

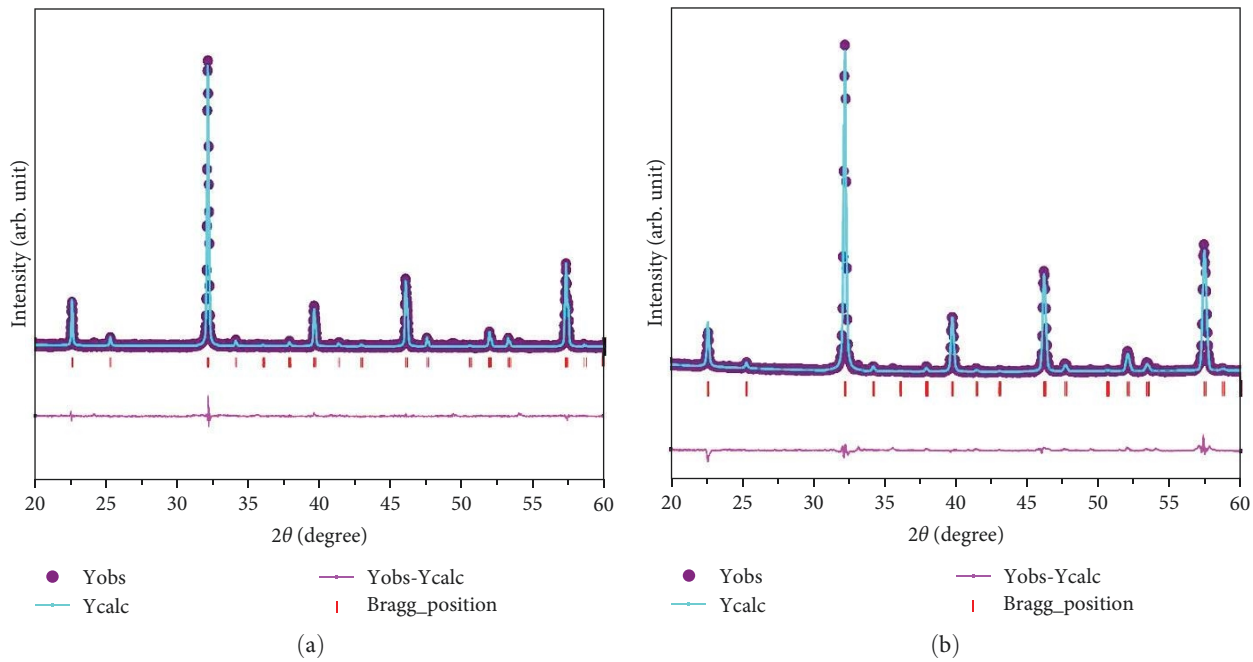

Figure 2: Graphical representations of the Rietveld refinement for the synthesized nanocrystalline materials: (a) $LaFeO_3$ and (b) $La_{0.5}Pr_{0.5}FeO_3$ ferrite materials.

Table 1: The refined structural parameters of the $LaFeO_3$ and $La_{0.5}Pr_{0.5}FeO_3$ ferrite materials.

Samples/parameters	$LaFeO_3$	$La_{0.5}Pr_{0.5}FeO_3$
a (Å)	5.559 (5)	5.564 (1)
b (Å)	5.569 (4)	5.566 (4)
c (Å)	7.860 (4)	7.859 (7)
Volume (Å^3)	242.75 (11)	312.42 (42)
R_{wp} (%)	3.8	3.6
R_p (%)	2.7	3.2
$\chi 2$	2.0	3.4
α (°)	90	90
β (°)	90	90
γ (°)	90	90
Crystallite size in (nm)	88	65
Fe–O bond length in (Å)	2.00	2.12
Minimum Fe–O bond length in (Å)	2.37	2.24
Maximum Fe–O bond length in (Å)	3.27	3.16

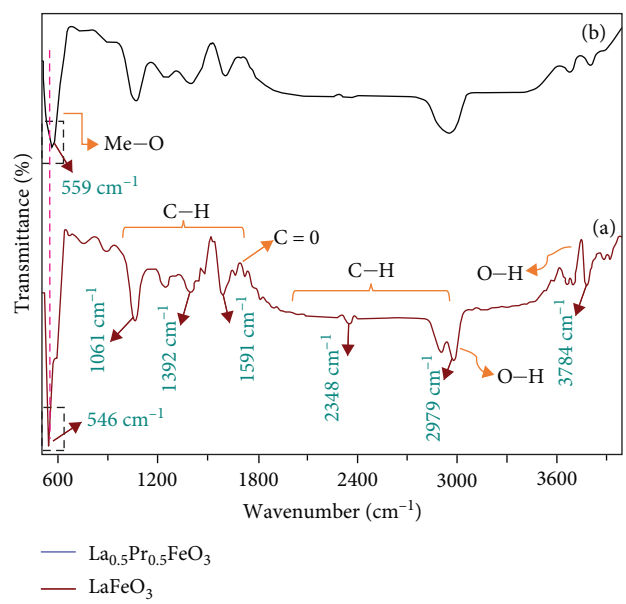

Figure 3: FT-IR spectra of synthesized nanocrystalline: (a) $LaFeO_3$ and (b) $La_{0.5}Pr_{0.5}FeO_3$ ferrite materials.

3.2. Fourier Transform-Infrared Spectroscopic (FT-IR) Studies. In Figure 3, the FT-IR spectra of the synthesized nanocrystalline LPFO materials within the wavelength range of 500–4000 cm^{-1} are depicted. Several notable features can be observed in these spectra. First, there is a prominent, intense band near 3000 cm^{-1}, which pertains to the stretching vibrational mode of O—H groups. This indicates the presence of hydroxyl (O—H) groups on the material's surface. Moreover, pristine LFO spectra indicate that the characteristic peaks are present at 1061, 1392, 1591, 2348, 2979, and 3784 cm^{-1}. Additionally, there is another band in the region of 1000–1600 cm^{-1}, which is attributed to the C—H bending vibrations. This indicates the presence of carbon–hydrogen bonds, likely originating from contaminants or impurities.

In the case of perovskite-type $LaFeO_3$, it adopts an orthorhombic structure wherein the crystal lattice's tetrahedral (A) and octahedral (B) positions are occupied by La^{3+} ions and Fe^{3+} ions, respectively. Typically, higher frequency bands in the region of 550–600 cm^{-1} and lower frequency bands in the region of 400–450 cm^{-1} are indicative of FeO and La—O bonds [25]. In this context, the FT-IR spectra

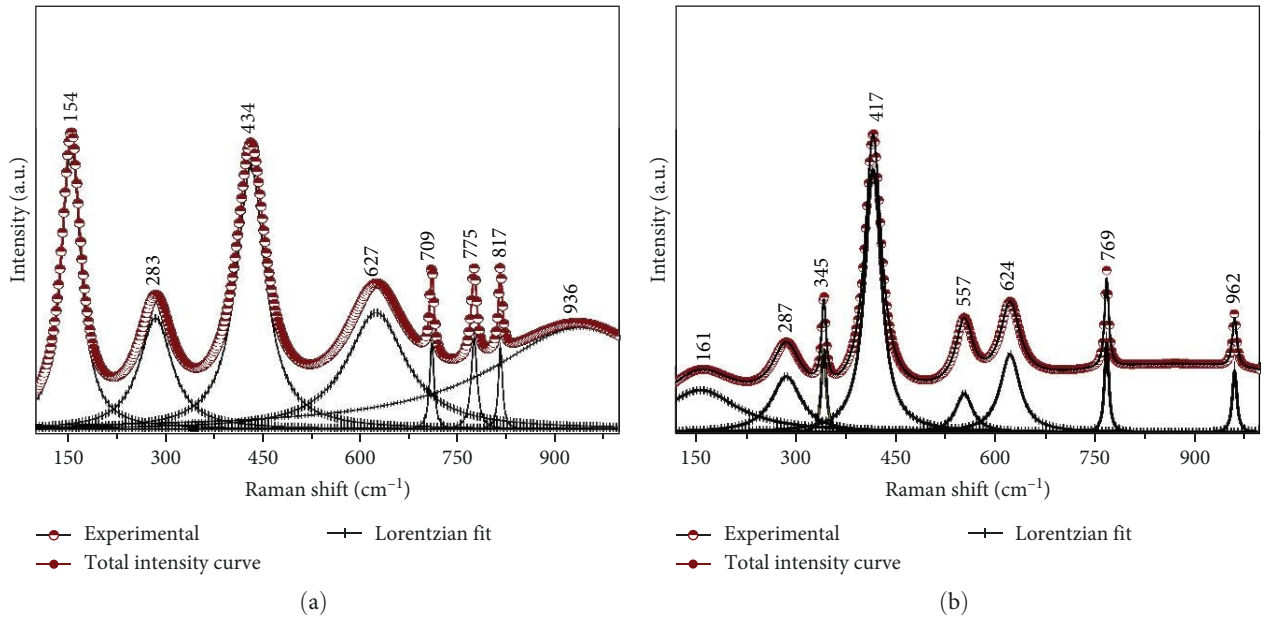

Figure 4: Raman peaks with a Lorentzian peak fit profile for the synthesized nanocrystalline $La_{1-x}Pr_xFeO_3$ ($x = 0.0$ and 0.5) ferrite materials. (a) $LaFeO_3$ and (b) $La_{0.5}Pr_{0.5}FeO_3$.

reveal bands at 546 and 559 cm^{-1}, which can be attributed to the intrinsic vibrations of the transition metal (TM) Fe—O complexes in synthesized both $LaFeO_3$ and $La_{0.5}Pr_{0.5}FeO_3$ materials. However, it is evident that there are slight variations in the intensity and position of these transition metal bands when rare-earth (Pr^{3+}) ions are substituted into lanthanum ferrites. These differences may arise from tiny variations in the crystal lattice, as indicated by the powder XRD results. This suggests that the substitution of Pr^{3+} ions influences the material's vibrational properties, reflecting changes in its crystal structure.

3.3. Raman Spectroscopy Analysis. Raman spectroscopic technique is a resilient tool for analyzing various aspects of materials, including impurity phases, cation distribution, spin–phonon coupling, crystal structure, and dynamical/local lattice distortion. Moreover, in the context of orthorhombic crystal structure, there exists a total of 60 vibrational modes within the Brillouin zone's center. However, only 24 of these modes (comprising $7A_g$, $5B_{1g}$, $7B_{2g}$, and $5B_{3g}$) are Raman active [26]. Figure 4 in the study presents the deconvolution of Raman peaks for $La_{1-x}Pr_xFeO_3$ ($x = 0.0$ and 0.5) using a Lorentzian profile fitting. In this figure, the blue lines denote the Lorentzian multipeak matching profile, the solid red curve denotes the sum of all the total intensity curves, and the black open circles depict the experimental data. Table 2 provides information on the various vibrational modes discovered through Raman spectroscopy, along with their probable attributes, based on the study of Watanabe et al. [27] and Sharma et al. [28].

According to the study, Raman spectroscopy is expected to reveal 24 modes with mixed symmetries in the Raman spectra of $La_{1-x}Pr_xFeO_3$ ($x = 0.0$ and 0.5). In the Raman analysis conducted, eight vibrational modes were identified, with the most intense mode appearing at 410–440 cm^{-1}. The table lists lower order frequencies below 900 cm^{-1}. For higher order frequencies, the mode at 930–970 cm^{-1} is attributed to oxygen stretching with $2A_{1g}(1)$ symmetry, while the mode at 936 cm^{-1} results from FeO_6 octahedra bending with $2A_{1g}(2)$ symmetry. Finally, the modes at 936 and 962 cm^{-1} possess A_{1g} symmetry and correspond to O_2 "scissors" and stretching movements, respectively. The presence of a few smaller peaks corresponding to B_g phonon modes and a decrease in the intensities of A_1 modes suggest that Pr^{3+} substitution has influenced the La-site in $LaFeO_3$. Raman scattering spectra are highly sensitive to atomic arrangements, and the observation of Raman active modes in $LaFeO_3$ ceramics provides valuable insights into the lattice structure alterations induced by Pr^{3+} substitution.

Table 2: Assignment of active Raman modes observed for $La_{1-x}Pr_xFeO_3$ ($x = 0.0$ and 0.5).

Raman modes (cm^{-1})	
$LaFeO_3$	$La_{0.5}Pr_{0.5}FeO_3$
154—A_{1g}	161—A_{1g}
283—B_{1g}	287—B_{1g}
434—A_{2g}	345—A_{2g}
627—B_{2g}	417—B_{2g}
709—B_{3g}	557—B_{3g}
775—A_{3g}	624—B_{4g}
817—B_{4g}	769—A_{3g}
936—$2A_{1g}$	962—$2A_{1g}$

3.4. Morphology Studies. Figure 5 displays SEM and TEM images of the synthesized nanocrystalline LPFO materials. Notably, the particles exhibit a nanoscale dimension, measuring less than 100 nm, and display a spherical shape. Furthermore, there is a tendency for these nanoparticles to

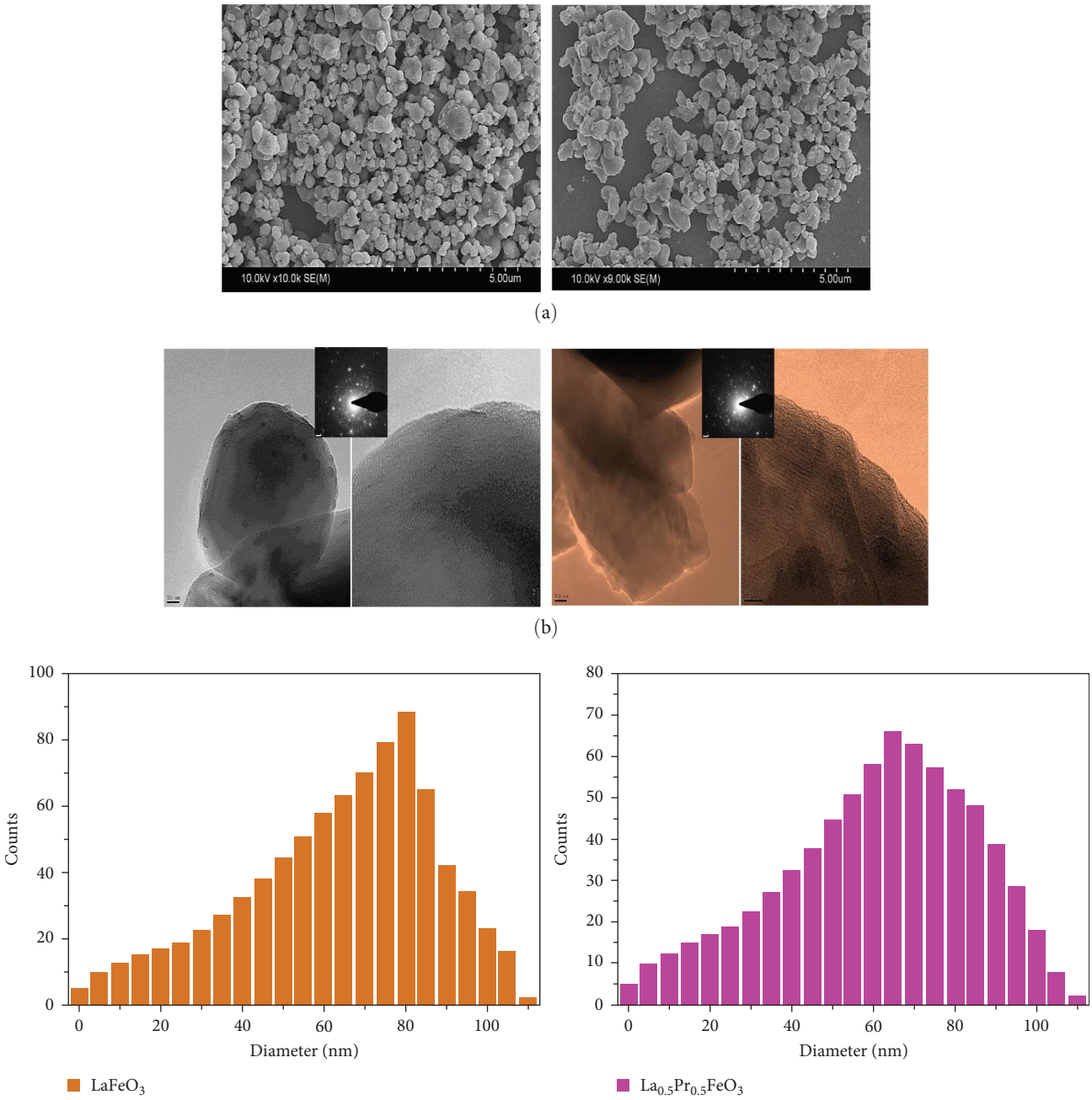

FIGURE 5: (a–c) SEM, TEM images, and particle size distribution histogram graph of synthesized nanocrystalline (left) $LaFeO_3$ and (right) $La_{0.5}Pr_{0.5}FeO_3$ ferrite materials.

cluster together, forming slight agglomerations. This propensity for spherical morphology and agglomeration is attributed to the presence of rare-earth (Pr^{3+}) ion substitutions and the synthesis temperature.

3.5. Dielectric Analysis. Figure 6 illustrates the frequency-dependent behavior of the dielectric properties (ε' and $\tan\delta$)) of $La_{1-x}Pr_xFeO_3$ ceramic compounds with different compositions ($x = 0.0$ and 0.5) at various temperatures. $LaFeO_3$ is known for its exceptional dielectric characteristics. In the lower frequency range, the dielectric constant exhibited high values, but as the frequency increased, it gradually decreased before stabilizing within the frequency range of 10^3–10^6 Hz. This phenomenon can be attributed to the higher resistivity and greater energy requirements for electron hopping at lower frequencies, resulting in increased energy loss. Conversely, at higher frequencies, conductivity increased, and electron hopping demanded less energy, leading to a reduction in the dielectric loss factor. It is important to remember that variables like composition, structural homogeneity, and

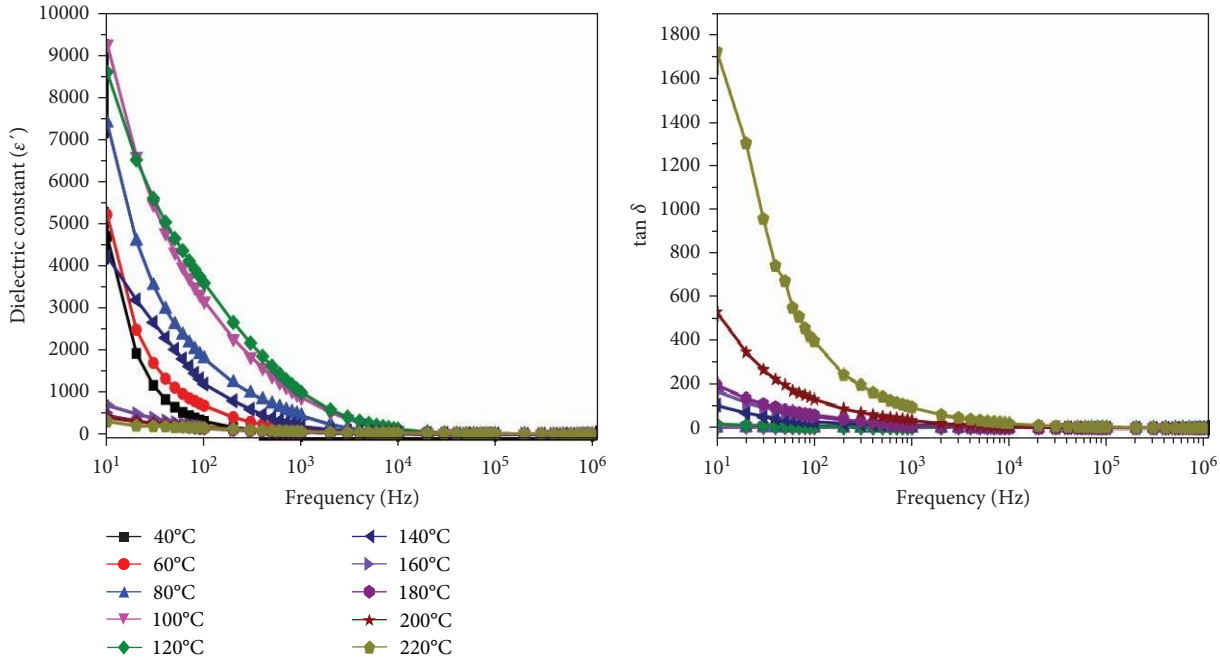

(a)

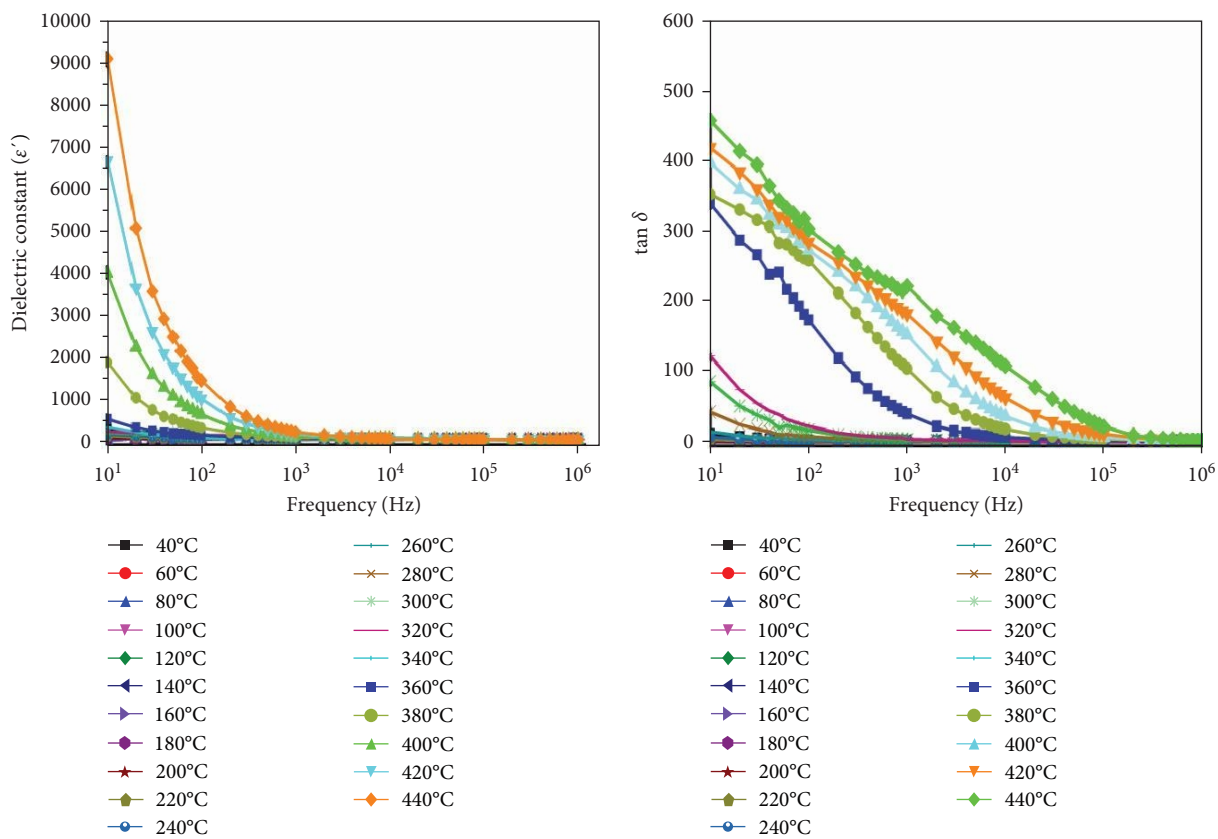

(b)

Figure 6: Frequency dependence dielectric constant and loss tangent of synthesized nanocrystalline $La_{1-x}Pr_xFeO_3$ ($x = 0.0$ and 0.5) ferrite materials. (a) $LaFeO_3$ and (b) $La_{0.5}Pr_{0.5}FeO_3$.

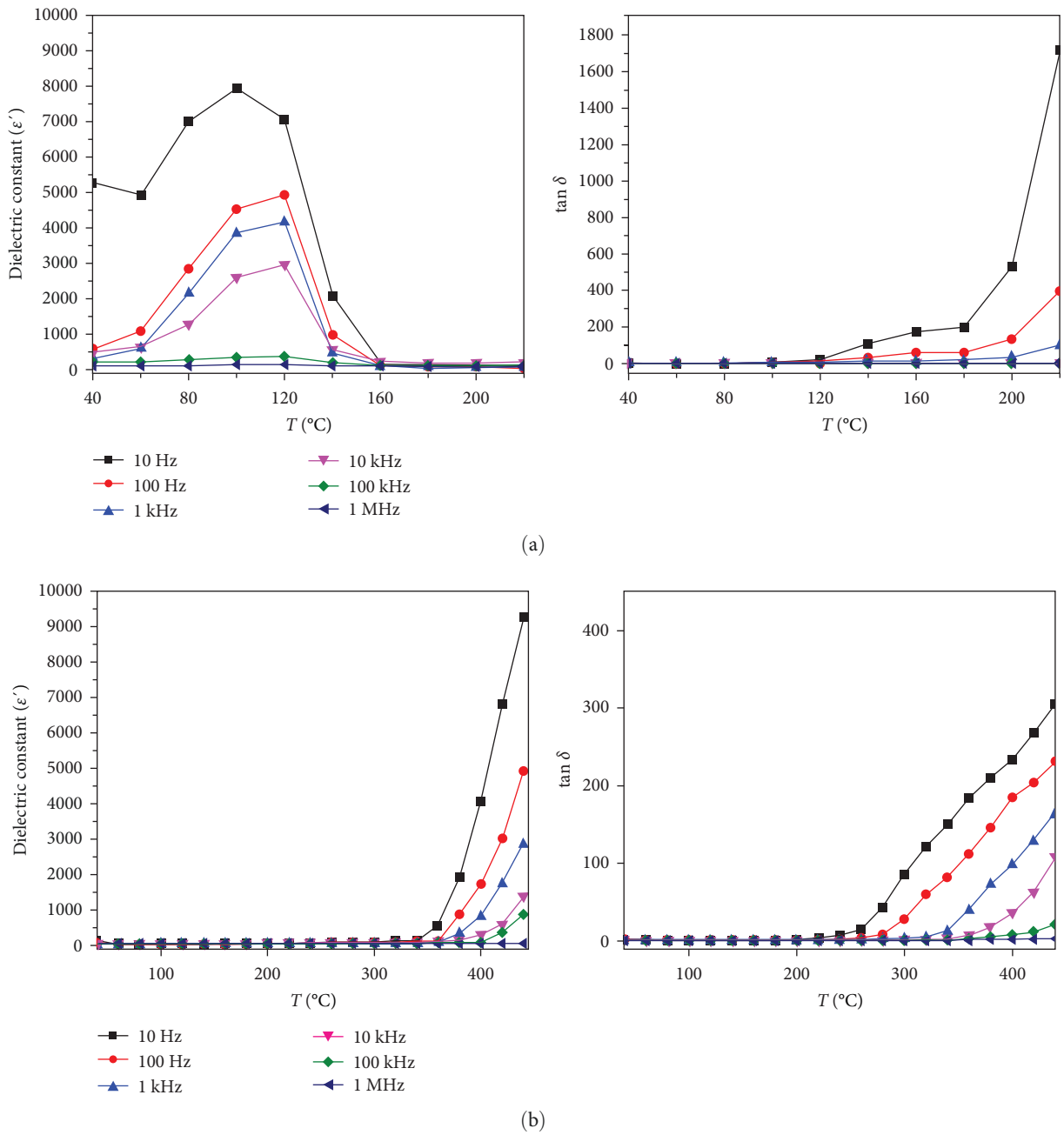

FIGURE 7: Temperature dependence dielectric constant and tangent loss of synthesized nanocrystalline $La_{1-x}Pr_xFeO_3$ ($x = 0.0$ and 0.5) ferrite materials. (a) $LaFeO_3$ and (b) $La_{0.5}Pr_{0.5}FeO_3$.

sintering temperature affect the dielectric loss factor. The findings revealed that as frequency increased, dielectric loss decreased in both samples [29].

Figure 7 displays the temperature-dependent characteristics of the dielectric properties (ε' and $\tan\delta$) for $La_{1-x}Pr_xFeO_3$ ceramic compounds with varying compositions ($x = 0.0$ and 0.5) at different frequencies. In this figure, it is evident that both pure and 0.5% praseodymium-substituted samples exhibit relatively low-dielectric loss factors. Additionally, at low temperatures ranging from 40 to 160°C, the dielectric constant decreases, while at higher temperatures, it increases, particularly at lower frequencies. The greater thermal energy at higher temperatures is blamed for this behavior, which enhances the mobility of charge carriers, leading to a higher hopping rate. Conversely, at low temperatures, thermal energy is insufficient to significantly contribute to charge carrier mobility, resulting in a decrease in the dielectric constant. This observed mechanism results in higher polarization at elevated temperatures, leading to an increase in the dielectric constant. Furthermore, both the ε' and $\tan\delta$ demonstrate relaxor behavior as the doping concentration increases. This behavior can be attributed to the chemical pressure

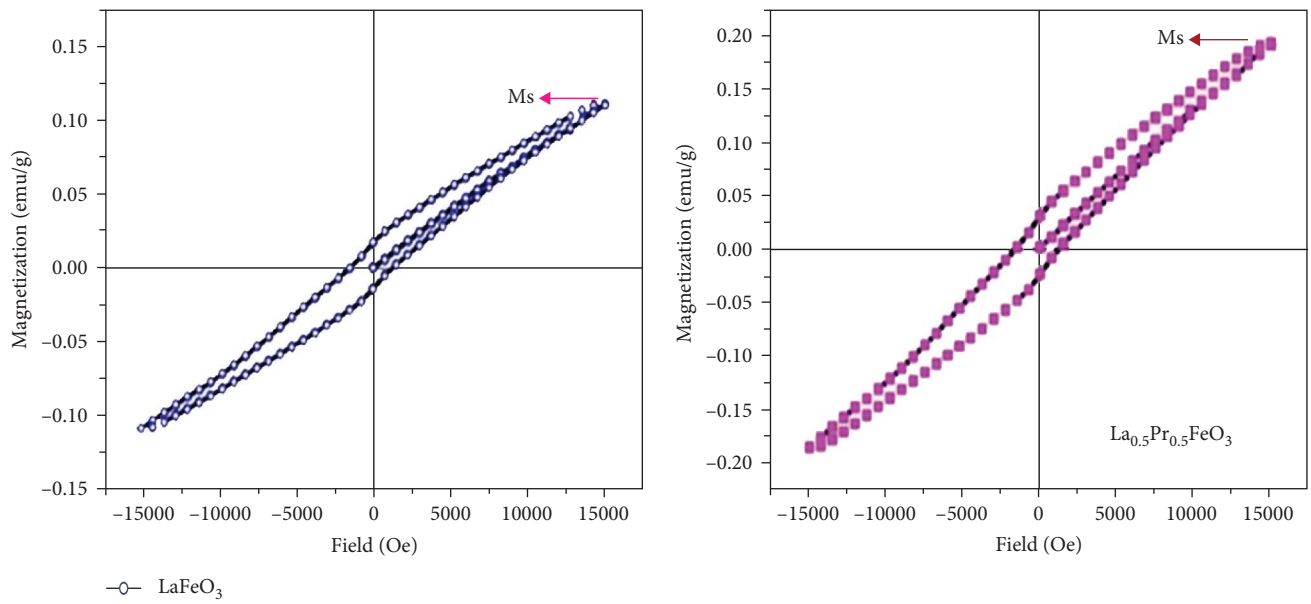

FIGURE 8: Hysteresis loops of synthesized nanocrystalline $La_{1-x}Pr_xFeO_3$ ($x = 0.0$ and 0.5) ferrite materials at room temperature.

induced in La–Fe–O due to the substitution of Pr^{3+} ions. These findings align with our most recent research findings [14].

3.6. Magnetic Analysis. The impact of Pr^{3+} doping on the magnetic characteristics of $LaFeO_3$ was explored using a vibrating sample magnetometer, as depicted in Figure 8. The magnetization hysteresis loop of the nanocrystalline $La_{1-x}Pr_xFeO_3$ ($x = 0.0$ and 0.5) ferrite materials, observed at room temperature, indicates that the prepared LPFO ferrite materials possess a soft nature and exhibit antiferromagnetic behavior since the synthesized materials were not saturated.

From the hysteresis loop, a number of significant parameters were recovered, including coercive field (Hc), magnetization at maximum field (±15 Oe) of the Pr^{3+} content ($x = 0.5$) in doped $LaFeO_3$ was exhibits both Ms (ranging from 0.108 to 0.19 emu/g at max. magnetic field) and Mr (varying from 0.01 to 0.027 emu/g) show an increase, while coercivity (decreasing from 1409.1 to 1325.6 Oe) decreases following the introduction of Pr^{3+} doping into $LaFeO_3$ ferrite materials synthesized via the traditional solid-state method.

This behavior can be elucidated by considering that the incorporation of rare-earth Pr^{3+} ions resulted in a reduction in crystallite size (as indicated in the XRD measurements). Consequently, this reduction disrupts the canted spins without compensation present at the surface and weakens the super–exchange interaction between Pr^{3+} ions and Fe ion (RE—O—RE, RE—O—Fe, and Fe—O—Fe, where RE represents rare-earth). It is worth noting that our results slightly deviate from the literature values, with Ms values reported as 0.6 emu/g for $LaFeO_3$, 0.5 emu/g for $La_{0.5}Nd_{0.5}FeO_3$, and 0.1 emu/g for $La_{0.5}Sm_{0.5}FeO_3$ [30, 31].

4. Conclusion

In an effort to modify the inherent properties of $LaFeO_3$ ferrite materials, Pr^{3+} doping (LPFO) was employed using the traditional solid-state method. This doping induced a lattice distortion, thereby allowing for the adjustment of the structural properties. FT-IR was used to analyze the creation of the crystal structure and the subsequent modifications in the bond stretching vibrations of tetrahedral and octahedral metal complexes. The introduction of Pr^{3+} dopants had a notable impact on the dielectric characteristics, particularly within the frequency span of 10 kHz–1 MHz and over the temperature variation of 40–160°C. The surface morphology of the materials was characterized as spherical with slight agglomeration. The room-temperature magnetic properties of the LPFO ferrite materials displayed antiferromagnetic behavior. Finally, it should be noted that the size of the crystallites had a significant impact on these magnetic properties, which resulted in a weakening of the super-exchange contact between Fe and Pr^{3+} ions.

Data Availability

No underlying data were collected or produced in this study

Conflicts of Interest

The authors declare that they have no conflicts of interest.

References

[1] H. Zhang, Z. Zeng, X. Shi, and Y. Du, "In-depth study on the structures and properties of rare-earth-containing perovskite materials," *Nanoscale*, no. 33, pp. 13976–13994, 2021.

[2] R. K. Raji, T. Ramachandran, M. Muralidharan et al., "Twitching the inherent properties: the impact of transition metal Mn-doped on $LaFeO_3$-based perovskite materials," *Journal of Materials Science: Materials in Electronics*, vol. 32, no. 20, pp. 25528–25544, 2021.

[3] S. K. Kundu, D. K. Rana, and L. Karmakar, "Enhanced multiferroic, magnetodielectric and electrical properties of Sm doped lanthanum ferrite nanoparticles," *Journal of Materials*

Science: Materials in Electronics, vol. 30, pp. 10694–10710, 2019.

[4] R. K. Raji, M. Muralidharan, T. Ramachandran et al., "Conventional synthesis of perovskite structured $LaTi_{x}$-$Fe_{1-x}O_3$: a comprehensive evaluation on phase formation, opto-magnetic, and dielectric properties," *International Journal of Materials Research*, vol. 112, no. 9, pp. 753–765, 2021.

[5] F. A. Fabian, P. P. Pedra, J. L. S. Filho, J. G. S. Duque, and C. T. Meneses, "Synthesis and characterization of La(Cr,Fe, Mn)O_3 nanoparticles obtained by co-precipitation method," *Journal of Magnetism and Magnetic Materials*, vol. 379, pp. 80–83, 2015.

[6] R. Abazari, S. Sanati, and L. A. Saghatforoush, "A unique and facile preparation of lanthanum ferrite nanoparticles in emulsion nanoreactors: morphology, structure, and efficient photocatalysis," *Materials Science in Semiconductor Processing*, vol. 25, pp. 301–306, 2014.

[7] W. Lee, H. Joong Yun, and J. Yoon, "Characterization and magnetic properties of $LaFeO_3$ nanofibers synthesized by electrospinning," *The Journal of Alloys and Compounds*, vol. 583, pp. 320–324, 2014.

[8] T. Fujii, I. Matsusue, D. Nakatsuka, M. Nakanishi, and J. Takada, "Synthesis and anomalous magnetic properties of $LaFeO_3$ nanoparticles by hot soap method," *Materials Chemistry and Physics*, vol. 129, pp. 805–809, 2011.

[9] S. Thirumalairajan, K. Girija, I. Ganesh et al., "Controlled synthesis of perovskite $LaFeO_3$ microsphere composed of nanoparticles via self-assembly process and their associated photocatalytic activity," *Chemical Engineering Journal*, vol. 209, pp. 420–428, 2012.

[10] S. Phokha, S. Pinitsoontorn, S. Rujirawat, and S. Maensiri, "Polymer pyrolysis synthesis and magnetic properties of $LaFeO_3$ nanoparticles," *Physica B*, vol. 476, pp. 55–60, 2015.

[11] Z. Wang, R. Gao, X. Deng, G. Chen, W. Cai, and C. Fu, "Dielectric and ferroelectric properties of $LaFeO_3$ particles derived from metal organic frameworks precursor," *Ceramics International*, vol. 45, pp. 1825–1830, 2019.

[12] M. A. Gabal, F. Al-Solami, Y. M. Al Angari et al., "Auto-combustion synthesis and characterization of perovskite-type $LaFeO_3$ nanocrystals prepared via different routes," *Ceramics International*, vol. 45, pp. 16530–16539, 2019.

[13] R. R. Kumar, T. Ramachandran, K. Natarajan, M. Muralidharan, F. Hamed, and V. Kurapati, "Fraction of rare-earth (Sm/Nd)-lanthanum ferrite-based perovskite ferroelectric and magnetic nanopowders," *Journal of Electronic Materials*, vol. 48, no. 3, Article ID 1694, 2019.

[14] R. K. Raji, K. Vishista, T. Ramachandran et al., "Tweaking the red emission, magneto, and dielectrical properties of perovskite type-$LaFeO_3$ in the presence of Co substitution," *Journal of Materials Science: Materials in Electronics*, vol. 31, pp. 7998–8014, 2020.

[15] N. Karthikeyan, R. R. Kumar, G. Jaiganesh, and K. Sivakumar, "Thermoelectric power factor of $La_{0.9}M_{0.1}FeO_3$ (M = Ca and Ba) system: structural, band gap and electrical transport evaluations," *Physica B: Condensed Matter*, vol. 529, pp. 1–8, 2018.

[16] M. Kumar, A. Kumar, S. Sharma et al., "Investigations on low temperature magnetic and magnetoelectric properties of multiferroic-NiO nanocomposites," *Journal of Alloys and Compounds*, vol. 965, Article ID 171353, 2023.

[17] M. U. Reygadas, S. Sharma, M. P. C. Manish Kumar, J. M. Siqueiros, O. R. Herrera, and B. Part, "Stability and physical properties of the K, Na and Nb doped $BiFeO_3$ lead-free system synthesized by the solid state route," *Ceramics International*, vol. 49, no. 17, pp. 28720–28728, 2023.

[18] A. Raj, M. Kumar, A. Kumar et al., "Comparative analysis of 'La' modified $BiFeO_3$-based perovskite solar cell devices for high conversion efficiency," *Ceramics International*, vol. 49, no. 1, pp. 1317–1327, 2023.

[19] M. Kumar, S. Sharma, O. Raymond-Herrera, and J. Siqueiros, "Investigations on dielectric, transport, and ferroelectric properties of Ca-modified $Bi_{0.80}La_{0.20}FeO_3$ ceramic synthesized by solid state reaction route," *Journal of Electronic Materials*, vol. 52, pp. 4312–4320, 2023.

[20] A. A. Saad, W. Khan, P. Dhiman, A. H. Naqvi, and M. Singh, "Structural, optical and magnetic properties of perovskite $(La_{1-x}Sr_x)(Fe_{1-x}Ni_x)O_3$," *Electronic Materials Letters*, vol. 9, no. 1, pp. 77–81, 2013.

[21] A. A. Saad, W. Khan, P. Dhiman, A. H. Naqvi, and M. Singh, "Redispersion of exsolved Cu nanoparticles on $LaFeO_3$ photocatalyst for tunable photocatalytic CO_2 reduction," *Chemical Engineering Journal*, vol. 452, no. Part 3, Article ID 139273, 2023.

[22] A. Hassan, W. Khan, S. Husain, P. Dhiman, M. Singh, and M. G. Alanazi, "Influence of Ni doping on physical properties of $La_{0.7}Sr_{0.3}FeO_3$ synthesized by reverse micelle technique," *Journal of Materials Science: Materials in Electronics*, vol. 32, pp. 3753–3765, 2021.

[23] R. Tholkappiyan, T. Thiemann, and F. Hamed, "Phase evolution and magnetic properties of $Dy_3Fe_{5+x}O_{12-x}$ nanocrystalline powders: a choice of fuel approach," *Materials Chemistry and Physics*, vol. 240, p. 122138, 2020.

[24] A. Muiruri, M. Maringa, and W. du Preez, "Evaluation of dislocation densities in various microstructures of additively manufactured Ti_6Al_4V (Eli) by the method of X-ray diffraction," *Materials*, vol. 13, no. 23, Article ID 5355, 2020.

[25] G. V. S. Rao, C. N. R. Rao, and J. R. Ferraro, "Infrared and electronic spectra of rare earth perovskites: ortho-chromites, manganites and -ferrites," *Applied Spectroscopy*, vol. 24, no. 4, pp. 436–445, 1970.

[26] D. L. Rousseau, P. Bauman, and P. S. Porto, "Normal mode determination in crystals," *Journal of Raman Spectroscopy*, vol. 10, no. 1, pp. 253–290, 1981.

[27] N. Watanabe, S. Adachi, S. Tajima, H. Yamauchi, and N. Koshizuka, "Phonon Raman scattering in polycrystalline Yt, $PrBazCu_{40}s$," *Physical Review B*, vol. 48, Article ID 6, 1993.

[28] P. Sharma, S. S. Dinesh Varshney, and P. K. Gupta, "Effect of Pr substitution on structural and electrical properties of $BiFeO_3$ ceramics," *Materials Chemistry and Physics*, vol. 143, pp. 629–636, 2014.

[29] K. Sultan, M. Ikram, and K. Asokan, "Structural, optical and dielectric study of Mn doped $PrFeO_3$ ceramics," *Vacuum*, vol. 99, pp. 251–258, 2014.

[30] P. Blessington, V. Pazhanivelu, C. Jagadeeshwaran, M. Rathinasamy, P. M. Gazzali, and G. Chandrasekaran, "An analysis on structural and magnetic properties of $La_{1-x}RE_xFeO_3$ ($x = 0.0$ and 0.5, RE = Nd, Sm and Gd) nanoparticles," *Applied Physics A*, vol. 123, no. 1, Article ID 13, 2016.

[31] R. K. Raji, M. Muralidharan, T. Ramachandran et al., "Dual-phase formation in $LaFeO_3$ upon doping of rare-earth Dy^{3+}: struct–opto–dielectric–magnetic characteristics," *Journal of Materials Science: Materials in Electronics*, vol. 33, no. 2, pp. 10626–10644, 2022.